Double shock-flame interactions and the induced flame instabilities

Xu Zhang[1], Ting Shen[2], Huahua Xiao[1,*]
[1]State Key Laboratory of Fire Science, University of Science and Technology of China, Hefei, Anhui, China
[2]Midea Group Kitchen & Water Heater Appliance, Foshan, Guangdong, China

1 Introduction

Shock–flame interactions arise in a wide range of phenomena, including supernova explosions[1], industrial explosions[2], and inertial confinement fusion. Previous studies show that when a shock wave interacts with a flame, it can induce baroclinic torque and trigger Richtmyer–Meshkov instability(RMI) on the flame front [3], [4]. This instability can distort the flame, increase the flame surface area, and enhance the combustion rate[5]. Such instability is also critical for flame acceleration and the deflagration-to-detonation transition (DDT)[6]. Although single shock–flame interactions have been well studied[7], multiple shock–flame interactions, commonly encountered in practical systems [8], [9], have attracted relatively limited attention.

Current studies on multiple shock–flame interactions primarily focus on scenarios where an incident shock wave first interacts with a flame and, after reflecting from a wall, interacts with the flame again in a direction opposite to that of the initial shock[10]. For instance, two-dimensional numerical simulations by Ju et al.[11] revealed that flame deformation and the second reflected shock both influence vorticity generation and vortex structure. Zhu et al.[12] performed numerical simulations of an incident shock and a reflected shock interacting with a spherical premixed flame. Their results show that RMI governs the early flame evolution after the first impact, whereas chemical reactions assume a more dominant role in subsequent stages. Similarly, Jiang et al.[13] showed that repeated shock impacts progressively shift the dominant mechanism of flame evolution from RMI to chemical reaction. Bambauer et al.[14] found that after the first shock–flame interaction reduces flame thickness by about half, the second shock interaction generates substantially higher vorticity, leading to pronounced increases in flame area and perturbations. Relatively few studies have examined two consecutive shocks impinging on a flame from the same direction.

The purpose of this work is to study the evolution of the flame front interacting with two consecutive shocks and reveal the mechanisms underlying the generated flame instabilities. The two-dimensional(2D) fully compressible reactive Navier–Stokes equations are solved using a high-order numerical algorithm and adaptive mesh refinement (AMR). In addition, the effect of the time interval between the two shocks is also examined.

Correspondence to: xiaoh@ustc.edu.cn

2 Numerical method and physical model

The numerical simulations solve the 2D fully compressible reactive Navier–Stokes equations with a model of chemically reacting stoichiometric hydrogen-air mixture[15]. A simplified chemical-diffusion model(CDM)[16] is used to model the combustion. The reaction rate is defined as: $\omega = \mathrm{d}Y/\mathrm{d}t = -A\rho Y \exp(-E_a/RT)$, where A is the pre-exponential factor, ρ is the density, Y is the mass fraction of reactant, E_a is the activation energy, R is universal gas constant. The initial temperature and pressure are 293 K and 1.01325 × 10^5 Pa, respectively. The CDM parameters used are based on those described in[6]. A fifth-order WENO algorithm with HLLC Riemann solver[17]is used to solve the governing equations. The time integration is advanced by using a third-order Runge–Kutta algorithm. The computational grid is dynamically refined using adaptive mesh refinement.

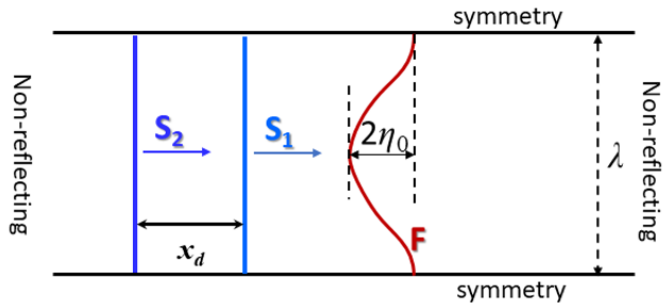

Figure 1: A snapshot of 2D computational domain. S_1: first shock; S_2: second shock; F: flame

As illustrated in Figure 1, the 2D computational domain is a rectangular region of width d and length 40d. Non-reflecting boundary conditions are imposed at the left and right boundaries, while the top and bottom boundaries are treated as symmetric walls. Post-shock gas parameters are prescribed according to the Rankine–Hugoniot relations and the specified Mach number. The initial flame perturbation is defined by $x = f(y) = (x_0 - \eta_0 \cos((y - \lambda/2) * 2\pi/\lambda))$, where ($x$, y) denotes the coordinates of the flame front. The domain width d is 1 cm, λ is the wavelength of the initial perturbation, η_0 is the perturbation amplitude, and x_0 is a constant indicating the flame's initial position within the domain. When the shock propagates from a burned region to an unburned region, the flame front constitutes a light/heavy configuration; conversely, it is classified as heavy/light.

Table 1 Operating Case Table.

Case	Number of Shock Impacts	Shock Spacing x_d (cm)	Time Interval Between Shocks Δt (μs)	Flame Front Type
1	Single	/	/	Light/Heavy
2	Double	4.2	27	Light/Heavy
3	Double	8	54	Light/Heavy
4	Double	12.4	85	Light/Heavy
5	Double	26	183	Light/Heavy
6	Single	/	/	Heavy/Light
7	Double	1.6	29	Heavy/Light
8	Double	2.8	56	Heavy/Light
9	Double	4	86	Heavy/Light
10	Double	8	182	Heavy/Light

3 Results

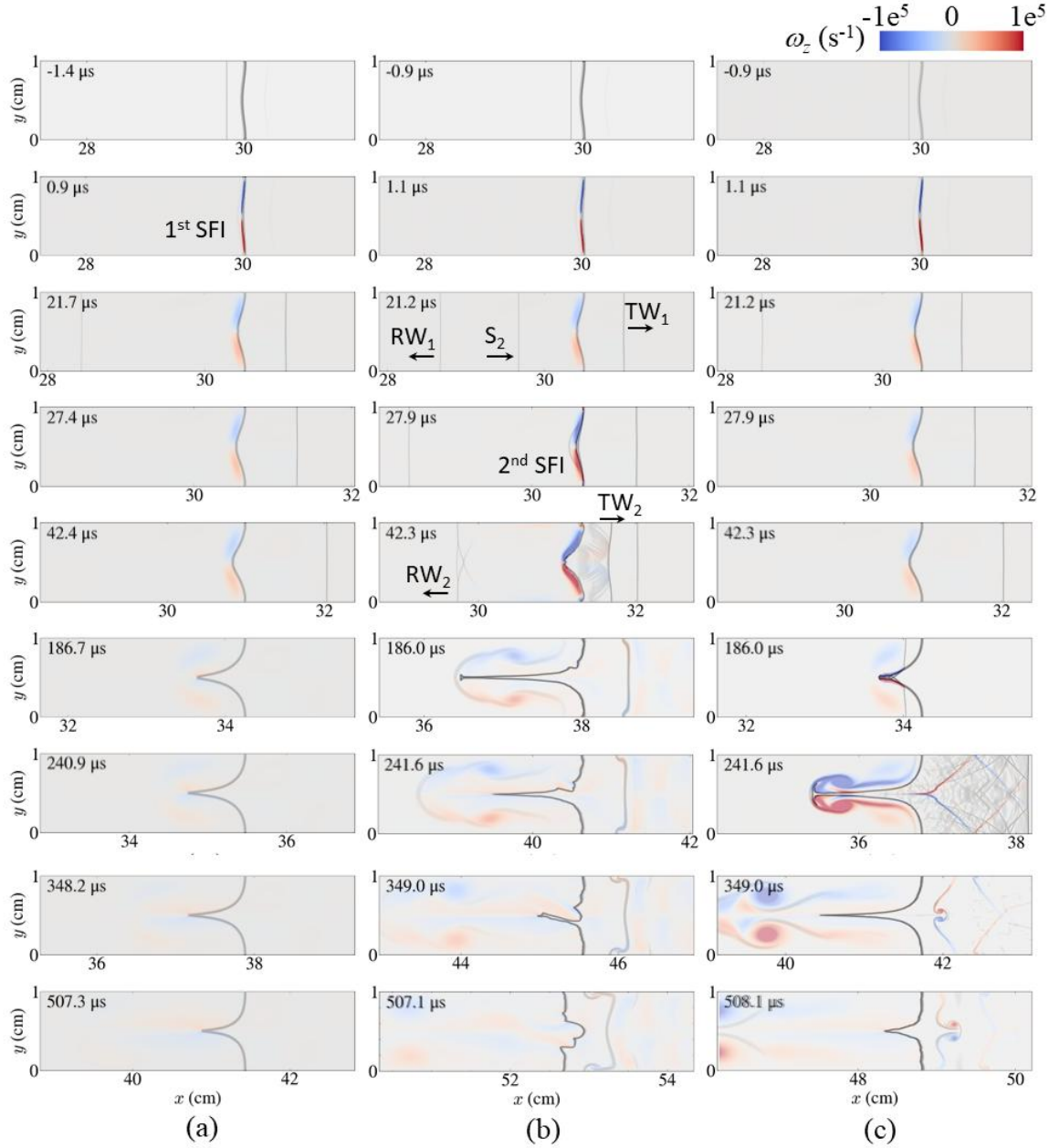

Figure 2: Schlieren and vorticity contour maps, (a) Case 1, (b) Case 2, (c) Case 5. TW: Transmitted shock; RW: reflected shock; SFI: first Shock–flame interactions

Figure 2 shows the schlieren and vorticity distributions in the vicinity of the flame front for Cases 1, 2 and 5, where t = 0 denotes the moment immediately before shock S_1 reaches the flame. As shown in Figure 2(a), the single shock–light/heavy flame interaction undergoes three distinct stages following the impact: (i) compression, (ii) perturbation growth, and (iii) flame-tip collapse. By contrast, when two shocks consecutively on the light/heavy flame, the flame front evolves through five stages: (i) compression, (ii) perturbation growth, (iii) compression, (iv) perturbation growth, and (v) flame-tip collapse (Figures 2(b) and 2(c)). In Case 2, shock S_1 penetrates the flame front, depositing vorticity of opposite signs on the upper and lower halves of the flame interface, with magnitudes on the order of $10^5 s^{-1}$(Figure 2(b) at 1.1 μs). During stage (i), the flame front is gradually compressed. In stage (ii), the

flame front begins to elongate after S_1 moves past. As shock S_2 arrives, the flame enters stage (iii), wherein the flame front is compressed again and acquires vorticity oriented similarly to that produced by S_1 (27.9 μs). At this point, transmitted shock TW_2 and reflected shock RW_2 also appear. Once S_2 departs, the flame transitions to stage (iv), characterized by renewed perturbation growth and the formation of minor wrinkles (42.3 μs). Subsequently, "spike" and "bubble" structures emerge (186.0 μs), with the spike region growing noticeably longer. As combustion proceeds, the upper and lower lips of the flame converge, culminating in flame-tip collapse during stage (v) (241.6 μs and 349.0 μs). Eventually, the flame evolves into a folded flame at 507.1 μs. A similar progression is observed in Case5.

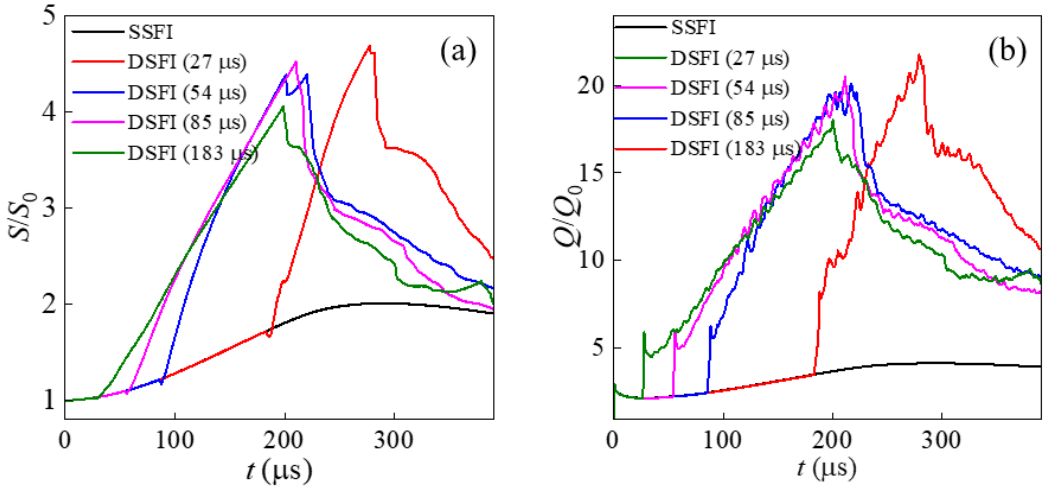

Figure 3: Normalised (a) flame surface area and (b) heat release rate as functions of time during the interaction of two consecutive shocks with a light/heavy flame at different Δt

Figure 3 shows the temporal evolution of the normalized flame area S/S_0 and the normalized heat release rate Q/Q_0 for Cases 1–5, where S and Q denote the instantaneous flame area and heat release rate, and S_0 and Q_0 are their initial values at t = 0. Under double shock–light/heavy flame interactions (DFSI), the second shock induces a decrease–increase–decrease pattern in the flame area. During shock S_2–induced compression, the heat release rate reaches its first peak. After S_2 exits, the rate increases once more but ultimately undergoes a sharp decline when the flame tip collapses. As illustrated in Figure 3, introducing the second shock raises the flame area to 2.2–2.5 times its single-shock value, while the peak heat release rate climbs to 4.3–4.7 times that of the single shock–flame interaction (SSFI). These enhancements grow more pronounced at larger Δt, indicating that the second shock interaction significantly promotes combustion.

Figure 4 shows the temporal evolution of the normalized flame area S/S_0 and the normalized heat release rate Q/Q_0 for Cases 6–10, illustrating double-shock heavy/light flame interactions. When $\Delta t \geqslant 56$ μs, the flame area follows a "decrease–increase–decrease" pattern, and the heat release rate exhibits two peaks before a sharp decline in the final stage. Under these conditions, the maximum flame area reaches 1.6–2.8 times the single-shock value, and the heat release rate increases by factors of 2.2–3.9. At this Δt , the second shock promotes combustion. By contrast, at Δt = 29 μs, the flame area initially decreases and then recovers after the second shock, yet the overall heat release rate remains below that of the single-shock case. At this smaller Δt, the second shock inhibits combustion This difference arises because, at small Δt, vorticity generated by the first interaction is not fully dissipated through combustion and diffusion, weakening the opposing vorticity produced by the second interaction and thereby slowing the subsequent growth of flame perturbations compared to the single-shock case.

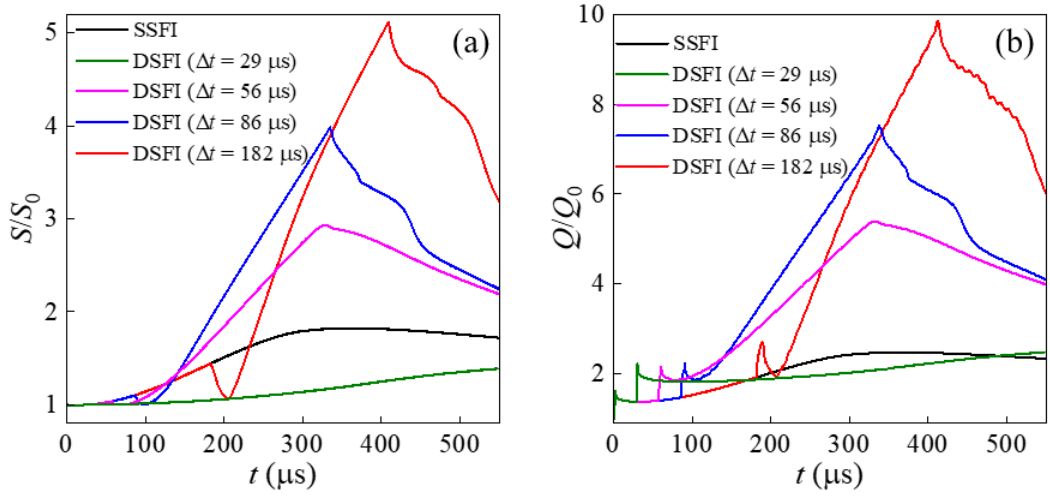

Figure 4: Normalised (a) flame surface area and (b) heat release rate as functions of time during the interaction of two consecutive shocks with a heavy/light flame at different Δt

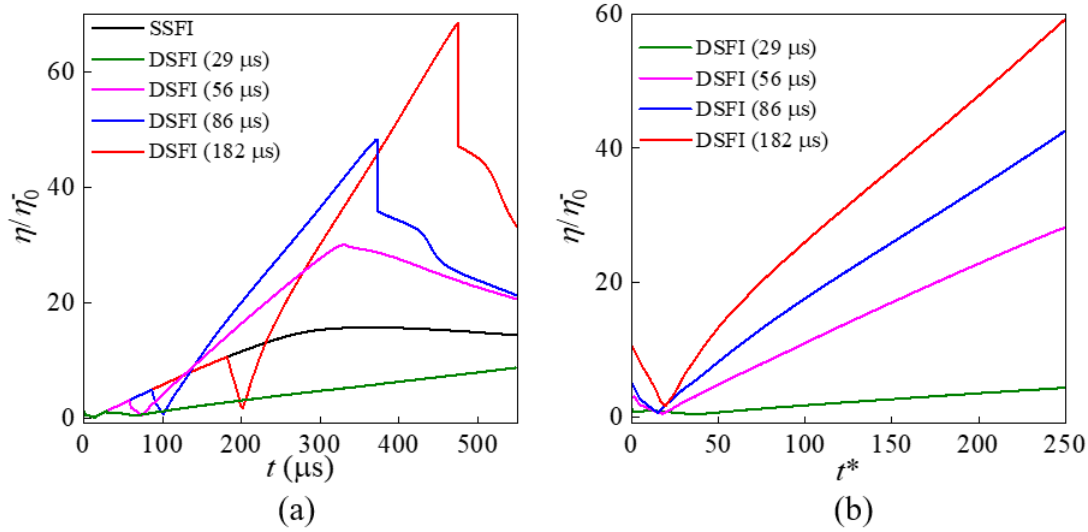

Figure 5: Temporal evolution of normalized flame perturbation amplitude (η/η_0^-) in double shock-heavy/light flame interactions: (a) complete timeline and (b) post second shock evolution ($t^* = t - \Delta t$)

4 Conclusions

The results show that, for the light/heavy cases, the flame instability progresses through five stages during the double shock interactions: compression, perturbation growth, secondary compression, enhanced perturbation growth, and flame-tip collapse. In this configuration, the second shock invariably enhances combustion for all Δt values through vorticity superposition, as both shock-flame interactions generate baroclinic vorticity with the same sign. By contrast, for the heavy/light cases, the second shock enhances combustion only when $\Delta t \geqslant 56$ μs. At shorter interval ($\Delta t = 29$ μs), the residual vorticity from the first shock-flame interaction has not been fully dissipated, and this results in partial cancellation of the newly generated opposing vorticity from the second interaction. This vorticity cancellation leads to significant weaker flame perturbation growth compared to the single shock case.

Acknowledgements

This work was supported by the Fundamental Research Funds for the Central Universities (Grant No. WK2320000061). We acknowledge the computing resources provided by the Supercomputing Center of University of Science and Technology of China (USTC).

References

[1] Poludnenko, AY. Chambers, J. Ahmed, K. and others. (2019). "A unified mechanism for unconfined deflagration-to-detonation transition in terrestrial chemical systems and type Ia supernovae." *Science*. 366: eaau7365.
[2] Oran, ES and Gamezo, VN. (2007). "Origins of the deflagration-to-detonation transition in gas-phase combustion." *Combustion and Flame*. 148: 4–47.
[3] Zhou, Y. (2017). "Rayleigh–Taylor and Richtmyer–Meshkov instability induced flow, turbulence, and mixing. I." *Physics Reports*. 720–722: 1–136.
[4] Zhou, Y. Williams, RJR. Ramaprabhu, P. and others. (2021). "Rayleigh–Taylor and Richtmyer–Meshkov instabilities: A journey through scales." *Physica D: Nonlinear Phenomena*. 423: 132838.
[5] Khokhlov, AM. Oran, ES. Chtchelkanova, AY. and others. (1999). "Interaction of a shock with a sinusoidally perturbed flame." *Combustion and Flame*. 117: 99–116.
[6] Xiao, H. Shen, T. Si, T. and others. (2023). "Three-dimensional shock–flame interactions: effect of wall friction." *Combustion Theory and Modelling*. 1–19.
[7] Yang, H and Radulescu, MI. (2021). "Enhanced DDT mechanism from shock-flame interactions in thin channels." *Proceedings of the Combustion Institute*. 38: 3481–3495.
[8] Wei, H. Zhang, X. Zeng, H. and others. (2019). "Mechanism of end-gas autoignition induced by flame-pressure interactions in confined space." *Physics of Fluids*. 31: N/A.
[9] Wei, H. Zhao, J. Zhang, X. and others. (2019). "Turbulent flame–shock interaction inducing end-gas autoignition in a confined space." *Combustion and Flame*. 204: 137–141.
[10] Jiang, H. Dong, G. Chen, X. and others. (2016). "Numerical simulations of the process of multiple shock–flame interactions." *Acta Mechanica Sinica*. 32: 659–669.
[11] Ju, Y. Shimano, A. and Inoue, O. (1998). "Vorticity generation and flame distortion induced by shock flame interaction." *Proceedings of the Combustion Institute*. 27: 735–741.
[12] Zhu, Y. Yang, Z. Pan, Z. Zhang, P. and Pan, J. (2018). "Numerical investigation of shock-SF6 bubble interaction with different mach numbers." *Computers & Fluids*. 177: 78–86.
[13] Jiang, H. Dong, G. Chen, X. and others. (2016). "A parameterization of the Richtmyer–Meshkov instability on a premixed flame interface induced by the successive passages of shock waves." *Combustion and Flame*. 169: 229–241.
[14] Bambauer, M. Hasslberger, J. and Klein, M. (2020). "Direct Numerical Simulation of the Richtmyer–Meshkov Instability in Reactive and Nonreactive Flows." *Combustion Science and Technology*. 192: 2010–2027.
[15] Xiao, H. Houim, RW. and Oran, ES. (2015). "Formation and evolution of distorted tulip flames." *Combustion and Flame*. 162: 4084–4101.
[16] Kaplan, CR. Ozgen, A. and Oran, ES. "Chemical-Diffusive Models for Flame Acceleration and Transition to Detonation: Genetic Algorithm and Optimization Procedure," Aug. 31, 2017, *arXiv*: arXiv:1709.00096.
[17] Thornber, B. Mosedale, A. Drikakis, D. Youngs, D. and Williams, RJR. (2008). "An improved reconstruction method for compressible flows with low Mach number features." *Journal of Computational Physics*. 227: 4873–4894.